HHS Public Access

Author manuscript

*J Pathol*. Author manuscript; available in PMC 2018 January 01.

Published in final edited form as:

*J Pathol*. 2017 January ; 241(1): 91–103. doi:10.1002/path.4834.

# *Fgf10* deficiency is causative for lethality in a mouse model of bronchopulmonary dysplasia

**Cho-Ming Chao**[1,4], **Faady Yahya**[1], **Alena Moiseenko**[1], **Caterina Tiozzo**[2], **Amit Shrestha**[1], **Negah Ahmadvand**[1], **Elie El Agha**[1], **Jennifer Quantius**[1], **Salma Dilai**[1], **Vahid Kheirollahi**[1], **Matthew Jones**[1], **Jochen Wilhem**[1], **Gianni Carraro**[3], **Harald Ehrhardt**[4], **Klaus-Peter Zimmer**[4], **Guillermo Barreto**[5], **Katrin Ahlbrecht**[6], **Rory E. Morty**[6], **Susanne Herold**[1], **Rosanna G. Abellar**[7], **Werner Seeger**[1,6], **Ralph Schermuly**[1], **Jin-San Zhang**[9], **Parviz Minoo**[8], and **Saverio Bellusci**[9,10,1,*]

[1]Universities of Giessen and Marburg Lung Center (UGMLC), Excellence Cluster Cardio-Pulmonary System (ECCPS), Member of the German Center for Lung Research (DZL), Department of Internal Medicine II, Aulweg 130, 35392 Giessen, Germany.

[2]Division of Neonatology, Department of Pediatrics, Columbia University, New York, NY, USA

[3]Departments of Medicine and Biomedical Sciences, Lung and Regenerative Medicine Institutes, Cedars-Sinai Medical Center, Los Angeles, CA 90048, USA.

[4]University Children´s Hospital Gießen, Division of General Pediatrics and Neonatology, Justus-Liebig-University, Gießen, Germany, Member of the German Lung Center (DZL).

[5]LOEWE Research Group, Lung Cancer Epigenetic, Max Planck Institute for Heart and Lung Research, Member of the German Lung Center (DZL), 61231 Bad Nauheim, Germany.

[6]Department of Lung Development and Remodeling, Max Planck Institute for Heart and Lung Research, Member of the German Lung Center (DZL), 61231 Bad Nauheim, Germany.

[7]Department of Pathology and Cell Biology, Columbia University, New York, NY 10032, USA

[8]Department of Pediatrics, Division of Newborn Medicine, University of Southern California, Childrens Hospital Los Angeles, Los Angeles, CA 90027, USA.

[9]College of Life and Environmental Sciences, Wenzhou University, Wenzhou, Zhejiang 325027, China

[10]Developmental Biology and Regenerative Medicine Program, Saban Research Institute of Children's Hospital Los Angeles and University of Southern California, Los Angeles, CA 90027, USA.

## Abstract

[*]Correspondence to: Saverio Bellusci, Universities of Giessen and Marburg Lung Center (UGMLC), Department of Internal Medicine II, Aulweg 130, 35392, Giessen, Germany. Saverio.Bellusci@innere.med.uni-giessen.de.

**Conflict of interest statement:** The authors disclose that they have no conflict of interest.

**Authors contributions**

Concept and design: CMC, SB, PM, acquisition of data: CMC, CT, FY, AS, AM, EEA, VK, MJ, SD, JW, JQ, RGA, NA, analysis and interpretation: JW, SB, CMC, HE, KA, REM, SH, RS, GC, JSZ, GB, drafting and editing of the manuscript: CMC, SB, WS, PM, KPZ, CT, EEA, MJ. All authors read and approved the final manuscript.

Inflammation-induced FGF10 protein deficiency is associated with bronchopulmonary dysplasia (BPD), a chronic lung disease of prematurely born infants characterized by arrested alveolar development. So far, experimental evidence for a direct role of FGF10 in lung disease is lacking. Using the hyperoxia-induced neonatal lung injury as a mouse model of BPD, the impact of *Fgf10* deficiency in $Fgf10^{+/-}$ *versus* $Fgf10^{+/+}$ pups was investigated. In normoxia, no lethality of $Fgf10^{+/+}$ or $Fgf10^{+/-}$ pups was observed. By contrast, all $Fgf10^{+/-}$ pups died within 8 days of hyperoxic injury, with lethality starting at day 5, whereas $Fgf10^{+/+}$ pups were all alive. Lungs of pups from the two genotypes were collected on postnatal day 3 following normoxia or hyperoxia exposure for further analysis. In hyperoxia, $Fgf10^{+/-}$ lungs exhibited increased hypoalveolarization. Analysis by FACS of the $Fgf10^{+/-}$ *versus* control lungs in normoxia, revealed a decreased ratio of alveolar epithelial type II (AECII) cells over total Epcam-positive cells. In addition, gene array analysis indicated reduced AECII and increased AECI transcriptome signatures in isolated AECII cells from $Fgf10^{+/-}$ lungs. Such an imbalance in differentiation is also seen in hyperoxia and associated with reduced mature surfactant protein B and C expression. Attenuation of the activity of Fgfr2b ligands post-natally in the context of hyperoxia lead also to increased lethality with decreased surfactant expression. In summary, decreased *Fgf10* mRNA levels leads to congenital lung defects, which are compatible with postnatal survival, but which compromise the ability of the lungs to cope with sub-lethal hyperoxic injury. *Fgf10* deficiency affects quantitatively and qualitatively the formation of AECII cells. In addition, Fgfr2b ligands are also important for repair after hyperoxia exposure in neonates. Deficient AECII cells could be an additional complication for patients with BPD.

### Keywords

Fibroblast growth factor 10; bronchopulmonary dysplasia; AECII; differentiation; surfactant

## Introduction

Fibroblast Growth Factor 10 (FGF10) protein deficiency has been reported in patients with bronchopulmonary dysplasia (BPD) [1]. BPD is a chronic lung disease of prematurely born infants and remains a leading cause of morbidity and mortality. In humans, inflammation is known to increase risk for BPD [2], [3]. Inflammatory mediators activated by bacterial-derived lipopolysaccharides (LPS) such as NF-κB, SP1 and SP3 were found to inhibit *Fgf10* transcription in mouse lung explants [4, 5]. The inhibition of *Fgf10* expression is mediated by LPS receptors (toll-like receptor 2 and 4) activation. In the context of the immature lung, the bio- and barotrauma induced by inflammation, mechanical ventilation and oxygen toxicity are known to cause injury [6–9]. Due to advances in management and therapy, survival of premature infants has increased. The histological characteristics of BPD have also changed. The “old” BPD was characterized by emphysema, interstitial fibrosis and airway squamous metaplasia. The “new” BPD is thought to be a “developmental lung disease”, arising from arrested alveolar development resulting in hypoalveolization and dysmorphic microvasculature [10]. BPD treatment is a considerable burden on health care systems [11, 12].

While the evidence confirming the key role of *Fgf10* in embryonic lung development is strong [13, 14], comparatively less is known about the consequences of constitutive *Fgf10* insufficiency following lung injury. To demonstrate the effect of *Fgf10* deficiency for prenatal and postnatal lung development in normoxic conditions, we used a constitutive heterozygous $Fgf10^{+/-}$ mouse line. Lung morphometry and gene array were performed to identify changes in lung structure and global gene expression in $Fgf10^{+/-}$ *versus* $Fgf10^{+/+}$ wild type (WT) littermate lungs at E18.5. Because oxygen toxicity is one of the major risk factors contributing to BPD, we used the mouse hyperoxia-induced BPD phenocopy model (85% oxygen from P0 – P8) to investigate the impact of *Fgf10* deficiency. Surprisingly, all $Fgf10^{+/-}$ pups died within 8 days of hyperoxic injury. We therefore chose P3, a time point at which there was no observable lethality, to collect pups for further analysis consisting of lung morphometry, gene array, fluorescence activated cell sorting (FACS), immunofluorescence (IF), reverse transcriptase-quantitative polymerase chain reactions (RT-qPCR), and western blotting. We also used a double transgenic system in mice [15–19] to attenuate all Fgfr2b ligands post-natally in the context of hyperoxic injury. Our detailed analysis may be critical in designing therapies to prevent lung injury in neonates at risk for BPD and in adult lung disorders characterized by FGF10 deficiency.

## Methods

### Study approval

Animal studies: all experiments were performed in accordance with the National Institutes of Health Guidelines for the Use of Laboratory Animals. Animal experiments were approved by the Federal Authorities for Animal Research of the Regierungspraesidium Giessen, Hessen, Germany; protocols 105/2011.

### Mice

C57BL/6 mice were crossed to generate WT pups. $Fgf10^{+/-}$ mice were generated by crossing $Fgf10^{flox/flox}$ mice (*Fgf10*$^{tm1.2Sms}$*/J*, Jacksonlab stock 023729) with *CMV-Cre* mice (*B6.C-Tg(CMV-cre)1Cgn/J*, Jacksonlab stock 006054). The resulting $Fgf10^{+/-}$ mice (*Fgf10*$^{tm1.1Sms}$*/J)* were crossed for at least five generations with C57BL/6 mice to remove the CMV-Cre allele and establish the $Fgf10^{+/-}$ mice in the C57BL/6 background. $Fgf10^{+/-}$ and $Fgf10^{+/+}$ embryonic and postnatal mice were used (both males and females). The $Fgf10^{Lacz/-}$ embryos were previously generated [20] by crossing the $Fgf10^{Lacz/+}$ (*Fgf10*$^{Tg(Myl3-lacZ)24Buck}$ obtained from Dr. Robert Kelly, Marseille, France and maintained on the C57BL/6 background for at least 5 generations) with the $Fgf10^{+/-}$ mice previously described. The *Rosa26*$^{rtTA/+}$*; Tg(tet(o)sFgfr2b)/+* mice (*Gt(ROSA)26Sor*$^{Tm1.1(rtTA,EGFP)Nagy}$ *Tg(tet0-sFgfr2b)1Jaw/CHC*) were generated by crossing *Rosa26rtTA/+* (*Gt(ROSA)26Sor*$^{Tm1.1(rtTA,EGFP)Nagy}$) with *Tg(tet(o)sFgfr2b)/+* mice (*Tg(tet0-sFgfr2b)1Jaw/CHC*, obtained from Dr. Jeffrey Whitsett, Cincinnatti, USA). Mice were kept on the CD1 background for at least 5 generations. Both genders were used.

### Hyperoxia injury (BPD mouse model)

Newborn pups were subjected to hyperoxia (HOX; 85% $O_2$) injury from P0–P8 in a chamber (ProOx Model 110, Biospherix). To minimize oxygen toxicity and bias, nursing

dams were rotated every 24 h between normoxia (NOX) and HOX. Pups and dams received food and water *ad libitum*.

### Statistical analyses

Significance was determined by two-tailed Student's *t*-test using GraphPad PRISM statistical analysis software. Chi-square analysis (software R, package "survival") was used for the comparison of survival data of all hyperoxia-exposed litters. All data are presented as mean ± SEM. Values of $p<0.05$ were considered significant.

### Left lobe perfusion, alveolar morphometry, RNA extraction, RT-qPCR, isolation of primary AECII cells, microarray experiments, FACS, western blot

See supplementary materials and methods

The data from the microarray experiment are deposited in GEO and is available through the accession number GSE76302

## Results

### *Fgf10* expression is reduced upon hyperoxia (HOX) exposure in neonatal wild type (WT) lungs

The expression of *Fgf10* and associated *Fgf* genes belonging to the same *Fgf* subfamily (*Fgf1, Fgf3 and Fgf7*) that encode Fgf ligands acting via Fgfr2b (21) was assessed by RT-qPCR in the lungs of C57BL/6 WT pups at different time points during normal alveologenesis (between P0 and P35). When normalized to their respective values for the first time point collected (P0), the results indicated a decrease in *Fgf10* expression over time, while the genes encoding other Fgfr2b ligands were maintained at stable levels (Figure 1Aa). Compared to *Fgf10*, *Fgf1* and *Fgf7* showed higher levels of mRNA while *Fgf3* was generally present at lower levels (Figure 1Ab). Comparing the expression (normalized to the first time point collected, P2) of these ligand's mRNAs in HOX (85% $O_2$ from P0 onwards) revealed that *Fgf10* was the only one with significantly lower levels at P5 and P8 compared to NOX-exposed WT lungs (Figure 1Ac).

### *Fgf10*$^{+/-}$ newborn mice are indistinguishable from WT littermates in NOX, but display increased lethality following HOX injury

Considering the previously reported decreased FGF10 expression in human patients with BPD, we investigated whether *Fgf10* deficiency in mice could reproduce the clinical complications observed in BPD. We therefore crossed *Fgf10*$^{+/-}$ and WT mice and collected embryos at E12.5 (n=3 and n=4 for WT and *Fgf10*$^{+/-}$, respectively) and E18.5 (n=3 and n=7 for WT and *Fgf10*$^{+/-}$, respectively) and assessed levels of *Fgf10* mRNA in their lungs by RT-qPCR. The relative levels of *Fgf10* were 23.7% and 57.9% less at E12.5 ($p=0.04$) and E18.5 ($p=0.01$), respectively) in *Fgf10*$^{+/-}$ *versus* WT lungs (data not shown). *Fgf10*$^{+/-}$ (n=10) and WT (n=12) pups exposed to NOX between P0 and P8 (Figure 1B) were viable and without phenotypic differences (data not shown). Morphometric analysis of P3 lungs (Figure 1Cb,d *versus* a,c n=4 for each genotype) showed no significant differences between *Fgf10*$^{+/-}$ and WT for the mean linear intercept (MLI), airspace or septal wall thickness

(Figure 1Da–c). To mimic the BPD phenotype, newborn pups were subjected to HOX for up to 8 days (Figure 1E) (22) (See also supplementary material, Figure S1 for the validation of the BPD model). Figure 1E–H displays the results for the pups from two litters combined together (14 pups). Survival analysis showed that all WT mice (n=8) survived at day 8 while none of the *Fgf10*$^{+/-}$ experimental mice (n=6) were alive at this time point (Chi-squared tests on the Cox proportional hazards models (group membership as only predictor): *Fgf10*$^{+/-}$ *versus* WT: Chi$^2$: 11.6, $p$ <0.001 (1 d.f.)). A 50% lethality was observed already at P5, suggesting that lung damage starts earlier (Figure 1F). We therefore analysed WT and *Fgf10*$^{+/-}$ lungs at P3 during the course of HOX. Haematoxylin-eosin staining of *Fgf10*$^{+/-}$ lungs (n=4) revealed an abnormal phenotype compared to WT lungs (n=4), with enlarged alveolar sacs and thinner interalveolar walls (Figure 1Gb,d *versus* a,c). Morphometric analysis demonstrated significantly increased MLI and airspace (both $p$=0.001) as well as decreased septal wall thickness ($p$=0.039) (Figure 1Ha–c).

## *Fgf10*$^{+/-}$ lungs exhibit impaired morphometry at E18.5 associated with reduced FGF signalling and epithelial marker expression as well as increased TGFβ signalling and ECM protein expression

We examined the presence of potential lung defects in E18.5 *Fgf10*$^{+/-}$ embryos. We also used previously described *Fgf10*$^{(Lacz/-)}$ hypomorphic mutants [20]. These two lines exhibit 50% and 20% *Fgf10* expression compared to WT lungs, respectively. Figure 2Aa–c shows the histology of the E18.5 WT (n=3), *Fgf10*$^{+/-}$ (n=7), and *Fgf10*$^{(Lacz/-)}$ hypomorphic (n=3) lungs. Morphometric analyses (Figure 2B) indicated that *Fgf10*$^{+/-}$ lungs exhibited increased MLI and airspace with no change in septal wall thickness compared to WT. Interestingly, *Fgf10*$^{Lacz/-}$ hypomorphic lungs mostly showed increased septal wall thickness with moderately but significantly increased MLI. The reason for this difference is unclear. So far, our results show that at P3, there is no obvious difference between *Fgf10*$^{+/-}$ and *Fgf10*$^{+/+}$ in NOX. However, at E18.5, morphometric analyses reveal differences between the two genotypes. The cellular and molecular mechanisms involved in this apparent recovery from E18.5 to P3 are so far unknown. In order to further characterize the nature of the lung morphological differences between the three conditions, we isolated RNA from WT (n=3), *Fgf10*$^{+/-}$ (n=7) and *Fgf10*$^{Lacz/-}$ hypomorphic (n=3) E18.5 lungs and carried out transcriptome analyses. Our approach using two distinct types of *Fgf10* mutants exhibiting different *Fgf10* levels allowed us to identify the top 70 mRNAs (selected based on $p$-value), which were differentially regulated between *Fgf10*$^{Lacz/-}$ hypomorph and WT lungs and then to compare the expression of these genes between *Fgf10*$^{+/-}$ and WT lungs. The heat map in Figure 2Ca (see supplementary material, Figure S2 for greater magnification) shows that these mRNAs were indeed also similarly decreased or increased in *Fgf10*$^{+/-}$ versus WT lungs. The graph in Figure 2Cb summarizes the different cellular compartments and biological processes that are potentially affected based on the known function of the identified genes. Interestingly, the expected epithelial defects of *Fgf10* deficiency could, in part, be caused by the dysregulated expression of epithelium-specific genes, such as *lysophosphatidylcholine acyltransferase 1* (*Lpcat1*), *phosphatidylinositol-4-phosphate-5-kinase, type I, alpha* (*Pip5k1a*), *G-protein-coupled receptor 30* (*Gpr30*), *calpain 6* (*Capn6*) and *pleiotrophin (Ptn*). In particular, *Lpcat1* deficiency has been associated with neonatal death due to surfactant defects [23], while *Ptn* promotes proliferation of alveolar epithelial

type II (AECII) cells and prevents their differentiation into AECI [24]. In addition to those implicated in epithelial defects, we also identified changes in transcripts expressed in muscle, the immune system, nerves and the extracellular matrix (ECM) (Figure 2Cc). These results highlight, as a consequence of either direct or indirect effects of *Fgf10* on the different cellular compartments, potential defects of *Fgf10*$^{+/-}$ lungs. Next, we validated by RT-qPCR the changes in FGF signalling and the associated epithelial markers between *Fgf10*$^{+/-}$ and WT lungs at E18.5 (Figure 2Da,b). We found that mRNA levels of *Fgf10*, *Fgfr2b* and *Bmp4*, the latter a downstream target of FGF10 in the epithelium, were decreased (all statistically significant). An overall trend of decreasing expression was also observed for other epithelial marker mRNAs. *Epcam* levels were significantly reduced, supporting that alterations occur in the epithelial compartment, which is the main cellular target of Fgf10 signalling. As Fgf10 and Tgfβ1 play opposite roles during lung development, we also investigated the expression of genes involved in TGFβ signalling and the associated ECM (Figure 2Dc,d). We found significantly increased *Smad3*, *Smad7* and *IL-1b* levels, but no changes for *Tgfb1* and *Tgfb3*. Additionally, mRNA levels for different types of collagen (*Col1a1*, *Col1a2*, *Col3a1*, *Col5a2*) showed trends to increase. The increase in TGFβ signalling was confirmed by IF using phospho-SMAD3 antibodies (Supplementary material, Figure S3).

## Characterization of the response to oxygen injury in AECII cells isolated from the lungs of WT and *Fgf10*$^{+/-}$ mice

In order to identify the significant genes/pathways differentially affected in AECII cells by HOX *versus* NOX between *Fgf10*$^{+/-}$ and WT, we isolated AECII from *Fgf10*$^{+/-}$ and WT P3 lungs in NOX and HOX conditions and compared their transcriptomes (supplementary material, Figure S4). In particular, we carried out an interaction "HOX × genotype" analysis (Figure 3). The volcano plot identified a set of genes that are either up- or down-regulated (Figure 3A). Interestingly, the majority of differences between the genotypes occurred in the downregulated genes.

The top 100 regulated genes according to their *p*-values are represented in the corresponding heat maps (Figure 3Ba,b, see supplementary material, Figure S5 for greater magnification). We found a gene-set (located in the lower part of the array) whose expression was not drastically changed in HOX between the two genotypes (Figure 3Ba), but was differentially regulated in NOX conditions (Figure 3Bb). Furthermore, another gene-set downregulated in HOX (located in the top part of the array) was upregulated in NOX conditions. KEGG analysis revealed that the processes altered were almost all linked to the immune system, and were downregulated in mutant AECII cells (Figure 3C). These processes were: systemic lupus erythematous, staphylococcus aureus infection, antigen presentation, graft *versus* host disease, and autoimmune thyroid disease, amongst others. In order to assess the differentiation status of the isolated AECII cells in *Fgf10*$^{+/-}$ *versus* WT lungs, we analysed the expression of the previously reported signatures for AECII and AECI (25) in the arrays generated from these cells in both NOX (Figure 3D) and HOX conditions (Figure 3E) (See supplementary material, Figure S6 for greater magnification). In both conditions, we found a decrease in the AECII signature, with a corresponding increase in the AECI signature.

Figure 3F, comparing differential expression between genotypes in HOX *versus* NOX confirms the differential clustering of the signatures for AECI and AECII.

## *Fgf10*$^{+/-}$ lungs in the context of HOX exhibit decreased surfactant expression

Using western blotting (whole lung homogenates, n=4 for WT and n=3 for *Fgf10*$^{+/-}$ lungs at P3, Figure 4Aa,b) we quantified the protein expression of Fgf10, Fgfr2 (using an antibody which does not discriminate between the Fgfr2b versus the Fgfr2c isoform) and mature Sftpc and Sftpb. We noted significantly reduced expression of all these markers in *Fgf10*$^{+/-}$ *versus* WT (Figure 4Aa–f). A decrease in Sftpb expression was also supported by immunofluorescence (Figure 4Ba,b).

Next, we investigated by FACS the prevalence of total epithelial cells (using Epcam as a general marker), AECI (podoplanin (Pdpn)-positive), AECII (Sftpc-positive) and epithelial stem/progenitor cells (EpiSPC; Epcam$^{high}$ CD24$^{low}$). In NOX, we observed a significant decrease in the Epcam-positive fraction of cells in *Fgf10*$^{+/-}$ *versus* WT lungs (Figure 4Ca). Interestingly, we noted an increased proportion of AECI cells (Figure 4Cb) and decreased proportion of AECII cells (Figure 4Cc) in *Fgf10*$^{+/-}$ *versus* WT lungs. This defect is in addition to the previously described impaired differentiation of the AECII cells in *Fgf10*$^{+/-}$ *versus* WT P3 lungs (Figure 3F). Interestingly, the prevalence of EpiSPC was not different between *Fgf10*$^{+/-}$ and WT lungs (Figure 4Cd). Following hyperoxic injury, the ratio of epithelial cells (Epcam+/whole lung) in *Fgf10*$^{+/-}$ *versus* WT was no longer significant (Figure 4Ce). However, the quantitative imbalance in AECI ratio in *Fgf10*$^{+/-}$ *versus* WT remained (Figure 4Cf), while the AECII ratio in *Fgf10*$^{+/-}$ *versus* WT was no longer significant (Fig. 4Cg). As for NOX, no difference was observed in the ratio of EpiSPC cells in *Fgf10*$^{+/-}$ *versus* WT (Fig. 4Ch). Next, we assessed cell proliferation using IF for Ki67 (Figure 4D). In this analysis we did not discriminate between epithelium and mesenchyme. In NOX, we observed a trend towards increased proliferation in *Fgf10*$^{+/-}$ *versus* WT lungs (Figure 4Da–c). In HOX, a significant increase in Ki67-positive cells was observed in *Fgf10*$^{+/-}$ *versus* WT lungs (Figure 4Dd–f). To confirm this observation, we assessed by IF the ratio of Ki67+, Cdh1+ double-positive cells (over the total number of cells stained by DAPI) in NOX and HOX (supplementary material, Figure S7). No difference was seen in NOX, but in contrast, HOX triggered a significant increase in Ki67+, Cdh1+ double-positive cells ($p$=0.05, supplementary material, Figure S7b *versus* a). Supporting the FACS data, which indicated reduced epithelial cell abundance (Epcam+ cells) in *Fgf10*$^{+/-}$ *versus* WT lungs in NOX, we observed a reduction in the prevalence of Cdh1-positive cells in NOX in *Fgf10*$^{+/-}$ *versus* WT lungs ($p$=0.004, supplementary material, Figure S7Ac). As observed for the FACS data, the difference in epithelial cell fraction between the two genotypes was no longer seen in HOX (supplementary material, Figure S7Ad). Investigating changes in the mesenchyme revealed significant increases, in NOX, for the fractions of CD45-negative, CD31- negative, and Epcam-negative over total cells in *Fgf10*$^{+/-}$ *versus* WT lungs (supplementary material, Figure S7Ba). This difference in the fraction of mesenchymal cells between the two genotypes was no longer detected in HOX (supplementary material, Figure S7Bb). Measurement by FACS of the ratio of haematopoietic and endothelial cells (defined as CD45+, CD31+, Epcam-negative) showed no difference in NOX and HOX between *Fgf10*$^{+/-}$ and WT lungs at P3 (data not shown).

### Postnatal attenuation of Fgfr2b ligands in NOX, during the saccular/alveolar stage of lung development, does not cause lung structural defects or lethality

As no congenital mutation in the *FGF10* gene in patients with BPD has been reported so far. It is therefore likely that in BPD babies, the initial stages of lung development occur in the presence of normal levels of FGF10. To mimic this situation in a mouse model, we used a previously reported dominant negative soluble *Fgfr2b* expression approach (*Rosa26*$^{rtTA/+}$*;Tg(tet(O)sFgfr2b)/+* mice) to scavenge, in an ubiquitous and doxycycline-inducible manner, all the Fgfr2b ligands, thereby turning off Fgfr2b signalling [15–19, 26]. Using this approach, we disrupted Fgfr2b signalling (mediated by Fgf1, 3, 7 and 10 see Figure 1A) in the postnatal lung during the saccular and the beginning of the alveolar stages, between P0 and P8 (Figure 5A–D). In NOX, we observed no lethality (Figure 5B) and no structural defects (Figure 5C,D) between double-transgenic experimental lungs (DTG) and single-transgenic control lungs (STG). Similar results were observed upon exposure to doxycycline for a longer time period, from P0 to P105 (data not shown).

### Postnatal attenuation of Fgfr2b ligands in HOX, during the saccular/alveolar stage of lung development, leads to significant lethality

In order to investigate the impact of attenuation of Fgfr2b during neonatal hyperoxia lung injury, we exposed two litters (including littermate controls, total 15 pups) to NOX and HOX (P0–P8). In contrast to NOX, HOX induced lethality in 50% of the *Rosa26*$^{rtTA/+}$*;Tg(tet(O)sFgfr2b)/+* DTG experimental group beginning at P6 (Figure 5E,F; Chi-squared tests on the Cox proportional hazards models (group membership as only predictor): *Rosa26rtTA;tet(O)sFgfr2b* vs WT: Chi$^2$: 6.2, p=0.012 (1 d.f.)). Compared to *Fgf10*$^{+/-}$ neonatal mice, this lethality started one day later (see Figure 1F) and the lethality at P8 was less (100% *versus* 50% dead in *Fgf10*$^{+/-}$ *versus* DTG, respectively). Morphometry at P3 (Figure 5G,H) showed increased MLI (+19.3%, $p$=0.029) in the DTG compared with the STG group control. This increase, compared to the *Fgf10*$^{+/-}$ *versus* WT in HOX (Fig. 1Ha) (+68.2%, $p$=0.001), supports our conclusion that in HOX, DTG lungs exhibit a less severe phenotype than do *Fgf10*$^{+/-}$ lungs. The lungs of *Fgf10*$^{+/-}$ mice at P3 in HOX had quantitative defects (increased AECI, decreased AECII) as well as impaired AECII differentiation (reduced AECII signature, increased AECI signature) associated with reduced Sftpc expression, so we also carried out western blotting for Sftpc, as well as FACS analysis, to assess the total number of epithelial cells (using Epcam), AECI (Pdpn-positive) and AECII (Sftpc-positive) in DTG and STG P3 lungs in NOX and HOX (Figure 6). In NOX, we did not find any significant differences between DTG and STG lungs (Figure 6A,B). By contrast, in HOX, we observed a reduction in Sftpc expression (Figure 6C), suggesting defective AECII cells. However, FACS analysis failed to show a quantitative difference between DTG and STG mice for Epcam, AECI or AECII cell fractions (Figure 6D).

## Discussion

Fgf10 maintains undifferentiated the Sox9/Id2-positive cells present in the distal lung epithelium [27, 28]. These cells are mutipotent epithelial progenitor cells. Lineage tracing using *Id2-CreERT2* showed that they give rise to both bronchiolar and alveolar progenitors. Based on single cell transcriptome studies of the developing epithelium, the alveolar

progenitors represent a population of “bipotent progenitor cells”. These bipotent cells differentiate into either AECI or AECII cells. However, what controls their differentiation remains unknown. A gene signature characteristic of each cell type has been recognised. The bipotent progenitor cells exhibit both signatures [25]. Our results suggest that Fgf10 may play a key role in directing the differentiation of the bipotent progenitor cells towards the AECII lineage. This conclusion is based on the observation that while the epithelial compartment is decreased in *Fgf10*$^{+/-}$ lungs, the ratio of AECII cells (to Epcam-positive cells) is also decreased, while that of AECI cells is increased. Interestingly, *Fgf10* hypomorphic lungs, exhibiting around 20% of the WT *Fgf10* mRNA level, also show a pronounced defect in AECII cells [20], supporting a role for Fgf10 in the ontogeny of the AECII lineage. The role, in this differentiation process, of the other Fgfr2b ligands abundantly expressed in the lung (Fgf1 and Fgf7) is unclear and will also need to be addressed. The observation that surfactant production, which is AECII’s primary function, is compromised in *Fgf10*$^{+/-}$ in HOX supports our conclusion that AECII cells from *Fgf10*$^{+/-}$ lungs are deficient. Interestingly, the AECII cells of *Fgf10*$^{+/-}$ lungs are still capable of producing enough surfactant to allow normal lung function in NOX. However, following HOX, these cells are prematurely lost due to built-in developmental (differentiation) defects that remain to be defined The observed increase in epithelial proliferation and the FACS data from *Fgf10*$^{+/-}$ *versus* WT lungs upon HOX injury appears to indicate an attempt to replenish the failing AECII pool. This newly formed AECII cell pool arising from either AECII stem cells [29] or other still unidentified sources, are apparently not able to substitute in surfactant protein b and c production. Western blotting analysis at P3 clearly showed a significant decrease in Sftpc and Sftpb expression (Figure 4Aa and 4Ab). Decreased surfactant expression is likely a major contributor to the lethal phenotype upon injury. Impaired surfactant production following hyperoxia exposure in adult mice upon Fgfr2b ligand blocking was reported previously [30]. In neonatal lung injury, the present results support the role of Fgfr2b ligands in the repair process of the AECII cells, and the associated surfactant expression.

Genome-wide association studies did not associate single-nucleotide polymorphisms in the *FGF10* gene with BPD [31]. Constitutive mutations in *FGF10* therefore appear to be rare, or non-existent, in BPD patients. However, the reduction in FGF10, which is linked to inflammation, may be associated with some of the clinical manifestations.

Our transcriptome results suggest differences exist in the immune status of AECII cells in *Fgf10*$^{+/-}$ *versus* WT lungs. The role of FGF signalling in controlling inflammation is still controversial. In primary cultures of human airway epithelial cells, FGF7 decreases transcript abundance for many interferon-induced genes, which may attenuate the response of epithelial cells to inflammatory mediators [32] (see [33] for a review of the role of Fgf7 in the lung). Short-term over-expression of Fgf7 *in vivo*, 3 days prior to acute lung injury, is protective. However, Fgf7 exposure for 7 days or longer increases lung inflammation and injury, suggesting differential cytoprotective *versus* inflammatory effects of Fgf7, dependent on the duration of growth factor treatment [34]. To date, such negative inflammatory effects have not been reported for Fgf10. In the future, precise analysis of epithelial gene expression will be critical for a better understanding of the biological responses triggered by Fgf10 *versus* Fgf7. Fgf10 increases the recruitment of T-regulatory cells in the context of

bleomycin injury [35] and mobilizes lung-resident mesenchymal stem cells and protects against acute lung injury [36]. Whether these effects are triggered by Fgf10-mediated epithelial signals or by Fgf10 acting on these inflammatory/stem cells remains to be elucidated.

Our results are also of interest regarding ALSG (aplasia of lacrimal and salivary glands) or LADD (lacrimo-auriculo-dento-digital syndrome) patients (exhibiting *FGF10* or *FGFR2b* mutations). While these patients initially appear to have normal lung function, they develop chronic obstructive pulmonary disease [37]. This is likely associated with deficient repair of the epithelium upon injury. It still remains to be investigated whether this is due to developmental defects in the epithelial progenitors and/or insufficient postnatal FGF10 levels that compromise epithelial maintenance. One aspect is clear; these patients will likely be more prone to lung disease than the normal population. At a minimum, prophylactic, preventive measures should be considered for these “at risk” patients.

## Supplementary Material

Refer to Web version on PubMed Central for supplementary material.

## Acknowledgments

We would like to thank Kerstin Goth and Jana Rostkovius for managing and genotyping the mice used for experiments. We also thank Prof. Wellington Cardoso for the critical reading of this manuscript. PM acknowledges the support from the Hastings foundation. PM and SB acknowledge the NHLBI support (HL107307). SB was supported by grants from the Deutsche Forschungsgemeinschaft (BE4443/4-1 and BE4443/6-1), Landes-Offensive zur Entwicklung Wissenschaftlich-ökonomischer Exzellenz, the Universtätsklinikum Giessen Marburg, the University of Giessen Marburg Lung Center, the German Center for Lung Research (DZL) and COST (BM1201). SH was supported by the Deutsche Forschungsgemeinschaft (SFB1221, C05; SFB-TR84, B2; EXC147), the Universitätsklinikum Giessen & Marburg (UKGM, FOKOOPV), and the German Center for Lung Research (DZL). The funders had no role in study design, data collection and analysis, decision to publish, or preparation of the manuscript.

## References

1. Benjamin JT, Smith RJ, Halloran BA, Day TJ, Kelly DR, Prince LS. FGF-10 is decreased in bronchopulmonary dysplasia and suppressed by Toll-like receptor activation. American journal of physiology Lung cellular and molecular physiology. 2007; 292(2):L550–L558. PubMed PMID: 17071719. [PubMed: 17071719]
2. Watterberg KL, Demers LM, Scott SM, Murphy S. Chorioamnionitis and early lung inflammation in infants in whom bronchopulmonary dysplasia develops. Pediatrics. 1996; 97(2):210–215. [PubMed: 8584379]
3. Klinger G, Levy I, Sirota L, Boyko V, Lerner-Geva L, Reichman B, et al. Outcome of early-onset sepsis in a national cohort of very low birth weight infants. Pediatrics. 2010; 125(4):e736–e740. PubMed PMID: 20231184. [PubMed: 20231184]
4. Benjamin JT, Carver BJ, Plosa EJ, Yamamoto Y, Miller JD, Liu JH, et al. NF-kappaB activation limits airway branching through inhibition of Sp1-mediated fibroblast growth factor-10 expression. J Immunol. 2010; 185(8):4896–4903. PubMed PMID: 20861353; PubMed Central PMCID: PMCPMC4399641. [PubMed: 20861353]
5. Carver BJ, Plosa EJ, Stinnett AM, Blackwell TS, Prince LS. Interactions between NF-kappaB and SP3 connect inflammatory signaling with reduced FGF-10 expression. J Biol Chem. 2013; 288(21): 15318–15325. PubMed PMID: 23558680; PubMed Central PMCID: PMCPMC3663551. [PubMed: 23558680]

6. Allen J, Zwerdling R, Ehrenkranz R, Gaultier C, Geggel R, Greenough A, et al. Statement on the care of the child with chronic lung disease of infancy and childhood. American journal of respiratory and critical care medicine. 2003; 168(3):356–396. Epub 2003/07/31. PubMed PMID: 12888611. [PubMed: 12888611]
7. Baraldi E, Filippone M. Chronic lung disease after premature birth. The New England journal of medicine. 2007; 357(19):1946–1955. Epub 2007/11/09, PubMed PMID: 17989387. [PubMed: 17989387]
8. Jain D, Bancalari E. Bronchopulmonary dysplasia: clinical perspective. Birth Defects Res A Clin Mol Teratol. 2014; 100(3):134–144. PubMed PMID: 24578124. [PubMed: 24578124]
9. Stoll BJ, Hansen NI, Bell EF, Shankaran S, Laptook AR, Walsh MC, et al. Neonatal outcomes of extremely preterm infants from the NICHD Neonatal Research Network. Pediatrics. 2010; 126(3): 443–456. PubMed PMID: 20732945; PubMed Central PMCID: PMCPMC2982806. [PubMed: 20732945]
10. Jobe AJ. The new BPD: an arrest of lung development. Pediatric research. 1999; 46(6):641–643. Epub 1999/12/10. PubMed PMID: 10590017. [PubMed: 10590017]
11. El Mazloum D, Moschino L, Bozzetto S, Baraldi E. Chronic lung disease of prematurity: long-term respiratory outcome. Neonatology. 2014; 105(4):352–356. PubMed PMID: 24931329. [PubMed: 24931329]
12. Jacob SV, Coates AL, Lands LC, MacNeish CF, Riley SP, Hornby L, et al. Long-term pulmonary sequelae of severe bronchopulmonary dysplasia. The Journal of pediatrics. 1998; 133(2):193–200. Epub 1998/08/26. PubMed PMID: 9709705. [PubMed: 9709705]
13. Chao CM, El Agha E, Tiozzo C, Minoo P, Bellusci S. A breath of fresh air on the mesenchyme: impact of impaired mesenchymal development on the pathogenesis of bronchopulmonary dysplasia. Frontiers in medicine. 2015; 2:27. PubMed PMID: 25973420; PubMed Central PMCID: PMC4412070. [PubMed: 25973420]
14. El Agha E, Bellusci S. Walking along the Fibroblast Growth Factor 10 Route: A Key Pathway to Understand the Control and Regulation of Epithelial and Mesenchymal Cell-Lineage Formation during Lung Development and Repair after Injury. Scientifica. 2014; 2014:538379. PubMed PMID: 25298902; PubMed Central PMCID: PMC4178922. [PubMed: 25298902]
15. Al Alam D, El Agha E, Sakurai R, Kheirollahi V, Moiseenko A, Danopoulos S, et al. Evidence for the involvement of fibroblast growth factor 10 in lipofibroblast formation during embryonic lung development. Development. 2015; 142(23):4139–4150. PubMed PMID: 26511927. [PubMed: 26511927]
16. Danopoulos S, Parsa S, Al Alam D, Tabatabai R, Baptista S, Tiozzo C, et al. Transient Inhibition of FGFR2b-ligands signaling leads to irreversible loss of cellular beta-catenin organization and signaling in AER during mouse limb development. PLoS One. 2013; 8(10):e76248. PubMed PMID: 24167544; PubMed Central PMCID: PMCPMC3805551. [PubMed: 24167544]
17. MacKenzie B, Henneke I, Hezel S, Al Alam D, El Agha E, Chao CM, et al. Attenuating endogenous Fgfr2b ligands during bleomycin-induced lung fibrosis does not compromise murine lung repair. American journal of physiology Lung cellular and molecular physiology. 2015; 308(10):L1014–L1024. PubMed PMID: 25820524; PubMed Central PMCID: PMCPMC4437006. [PubMed: 25820524]
18. Parsa S, Kuremoto K, Seidel K, Tabatabai R, Mackenzie B, Yamaza T, et al. Signaling by FGFR2b controls the regenerative capacity of adult mouse incisors. Development. 2010; 137(22):3743–3752. Epub 2010/10/28. doi:137/22/3743 [pii]10.1242/dev.051672. PubMed PMID: 20978072; PubMed Central PMCID: PMC3049274. [PubMed: 20978072]
19. Parsa S, Ramasamy SK, De Langhe S, Gupte VV, Haigh JJ, Medina D, et al. Terminal end bud maintenance in mammary gland is dependent upon FGFR2b signaling. Dev Biol. 2008; 317(1): 121–131. Epub 2008/04/03. doi: S0012-1606(08)00110-3 [pii]10.1016/j.ydbio.2008.02.014. PubMed PMID: 18381212. [PubMed: 18381212]
20. Ramasamy SK, Mailleux AA, Gupte VV, Mata F, Sala FG, Veltmaat JM, et al. Fgf10 dosage is critical for the amplification of epithelial cell progenitors and for the formation of multiple mesenchymal lineages during lung development. Dev Biol. 2007; 307(2):237–247. PubMed PMID: 17560563; PubMed Central PMCID: PMCPMC3714306. [PubMed: 17560563]

21. Itoh N, Ornitz DM. Functional evolutionary history of the mouse Fgf gene family. Dev Dyn. 2008; 237(1):18–27. PubMed PMID: 18058912. [PubMed: 18058912]
22. Berger J, Bhandari V. Animal models of bronchopulmonary dysplasia. The term mouse models. American journal of physiology Lung cellular and molecular physiology. 2014; 307(12):L936–L947. PubMed PMID: 25305249; PubMed Central PMCID: PMCPMC4269689. [PubMed: 25305249]
23. Bridges JP, Ikegami M, Brilli LL, Chen X, Mason RJ, Shannon JM. LPCAT1 regulates surfactant phospholipid synthesis and is required for transitioning to air breathing in mice. The Journal of clinical investigation. 2010; 120(5):1736–1748. PubMed PMID: 20407208; PubMed Central PMCID: PMCPMC2860922. [PubMed: 20407208]
24. Weng T, Gao L, Bhaskaran M, Guo Y, Gou D, Narayanaperumal J, et al. Pleiotrophin regulates lung epithelial cell proliferation and differentiation during fetal lung development via beta-catenin and Dlk1. J Biol Chem. 2009; 284(41):28021–28032. PubMed PMID: 19661059; PubMed Central PMCID: PMCPMC2788854. [PubMed: 19661059]
25. Treutlein B, Brownfield DG, Wu AR, Neff NF, Mantalas GL, Espinoza FH, et al. Reconstructing lineage hierarchies of the distal lung epithelium using single-cell RNA-seq. Nature. 2014; 509(7500):371–375. PubMed PMID: 24739965; PubMed Central PMCID: PMC4145853. [PubMed: 24739965]
26. Volckaert T, Dill E, Campbell A, Tiozzo C, Majka S, Bellusci S, et al. Parabronchial smooth muscle constitutes an airway epithelial stem cell niche in the mouse lung after injury. The Journal of clinical investigation. 2011; 121(11):4409–4419. PubMed PMID: 21985786; PubMed Central PMCID: PMCPMC3204843. [PubMed: 21985786]
27. Volckaert T, Campbell A, Dill E, Li C, Minoo P, De Langhe S. Localized Fgf10 expression is not required for lung branching morphogenesis but prevents differentiation of epithelial progenitors. Development. 2013; 140(18):3731–3742. Epub 2013/08/09. PubMed PMID: 23924632; PubMed Central PMCID: PMC3754473. [PubMed: 23924632]
28. Nyeng P, Norgaard GA, Kobberup S, Jensen J. FGF10 maintains distal lung bud epithelium and excessive signaling leads to progenitor state arrest, distalization, and goblet cell metaplasia. BMC developmental biology. 2008; 8:2. PubMed PMID: 18186922; PubMed Central PMCID: PMC2263027. [PubMed: 18186922]
29. Barkauskas CE, Cronce MJ, Rackley CR, Bowie EJ, Keene DR, Stripp BR, et al. Type 2 alveolar cells are stem cells in adult lung. The Journal of clinical investigation. 2013; 123(7):3025–3036. PubMed PMID: 23921127; PubMed Central PMCID: PMC3696553. [PubMed: 23921127]
30. Hokuto I, Perl AK, Whitsett JA. FGF signaling is required for pulmonary homeostasis following hyperoxia. American journal of physiology Lung cellular and molecular physiology. 2004; 286(3):L580–L587. PubMed PMID: 14617521. [PubMed: 14617521]
31. Hadchouel A, Durrmeyer X, Bouzigon E, Incitti R, Huusko J, Jarreau PH, et al. Identification of SPOCK2 as a susceptibility gene for bronchopulmonary dysplasia. American journal of respiratory and critical care medicine. 2011; 184(10):1164–1170. PubMed PMID: 21836138. [PubMed: 21836138]
32. Prince LS, Karp PH, Moninger TO, Welsh MJ. KGF alters gene expression in human airway epithelia: potential regulation of the inflammatory response. Physiological genomics. 2001; 6(2): 81–89. [PubMed: 11459923]
33. Ware LB, Matthay MA. Keratinocyte and hepatocyte growth factors in the lung: roles in lung development, inflammation, and repair. American journal of physiology Lung cellular and molecular physiology. 2002; 282(5):L924–L940. PubMed PMID: 11943656. [PubMed: 11943656]
34. Tichelaar JW, Wesselkamper SC, Chowdhury S, Yin H, Berclaz PY, Sartor MA, et al. Duration-dependent cytoprotective versus inflammatory effects of lung epithelial fibroblast growth factor-7 expression. Experimental lung research. 2007; 33(8–9):385–417. PubMed PMID: 17994369. [PubMed: 17994369]
35. Gupte VV, Ramasamy SK, Reddy R, Lee J, Weinreb PH, Violette SM, et al. Overexpression of fibroblast growth factor-10 during both inflammatory and fibrotic phases attenuates bleomycin-induced pulmonary fibrosis in mice. American journal of respiratory and critical care medicine. 2009; 180(5):424–436. PubMed PMID: 19498056; PubMed Central PMCID: PMCPMC2742760. [PubMed: 19498056]

36. Tong L, Zhou J, Rong L, Seeley EJ, Pan J, Zhu X, et al. Fibroblast Growth Factor-10 (FGF-10) Mobilizes Lung-resident Mesenchymal Stem Cells and Protects Against Acute Lung Injury. Scientific reports. 2016; 6:21642. PubMed PMID: 26869337; PubMed Central PMCID: PMC4751498. [PubMed: 26869337]

37. Klar J, Blomstrand P, Brunmark C, Badhai J, Hakansson HF, Brange CS, et al. Fibroblast growth factor 10 haploinsufficiency causes chronic obstructive pulmonary disease. J Med Genet. 2011; 48(10):705–709. PubMed PMID: 21742743. [PubMed: 21742743]

38. McGrath-Morrow SA, Cho C, Soutiere S, et al. The effect of neonatal hyperoxia on the lung of p21Waf1/Cip1/Sdi1-deficient mice. Am J Respir Cell Mol Biol. 2004; 30:635–640. [PubMed: 14607813]

39. Woyda K, Koebrich S, Reiss I, et al. Inhibition of phosphodiesterase 4 enhances lung alveolarisation in neonatal mice exposed to hyperoxia. Eur Respir J. 2009; 33:861–870. [PubMed: 19010982]

40. Seimetz M, Parajuli N, Pichl A, et al. Inducible NOS inhibition reverses tobacco-smoke-induced emphysema and pulmonary hypertension in mice. Cell. 2011; 147:293–305. [PubMed: 22000010]

41. Gentleman RC, Carey VJ, Bates DM, et al. Bioconductor: open software development for computational biology and bioinformatics. Genome biology. 2004; 5:R80. [PubMed: 15461798]

42. Smyth GK. Linear models and empirical Bayes methods for assessing differential expression in microarray experiments. Stat Appl Genet Mol Biol. 2004; 3 Article3.

43. McQualter JL, Yuen K, Williams B, et al. Evidence of an epithelial stem/progenitor cell hierarchy in the adult mouse lung. Proc Natl Acad Sci U S A. 2010; 107:1414–1419. [PubMed: 20080639] * These references are cited exclusively in supplementary material online

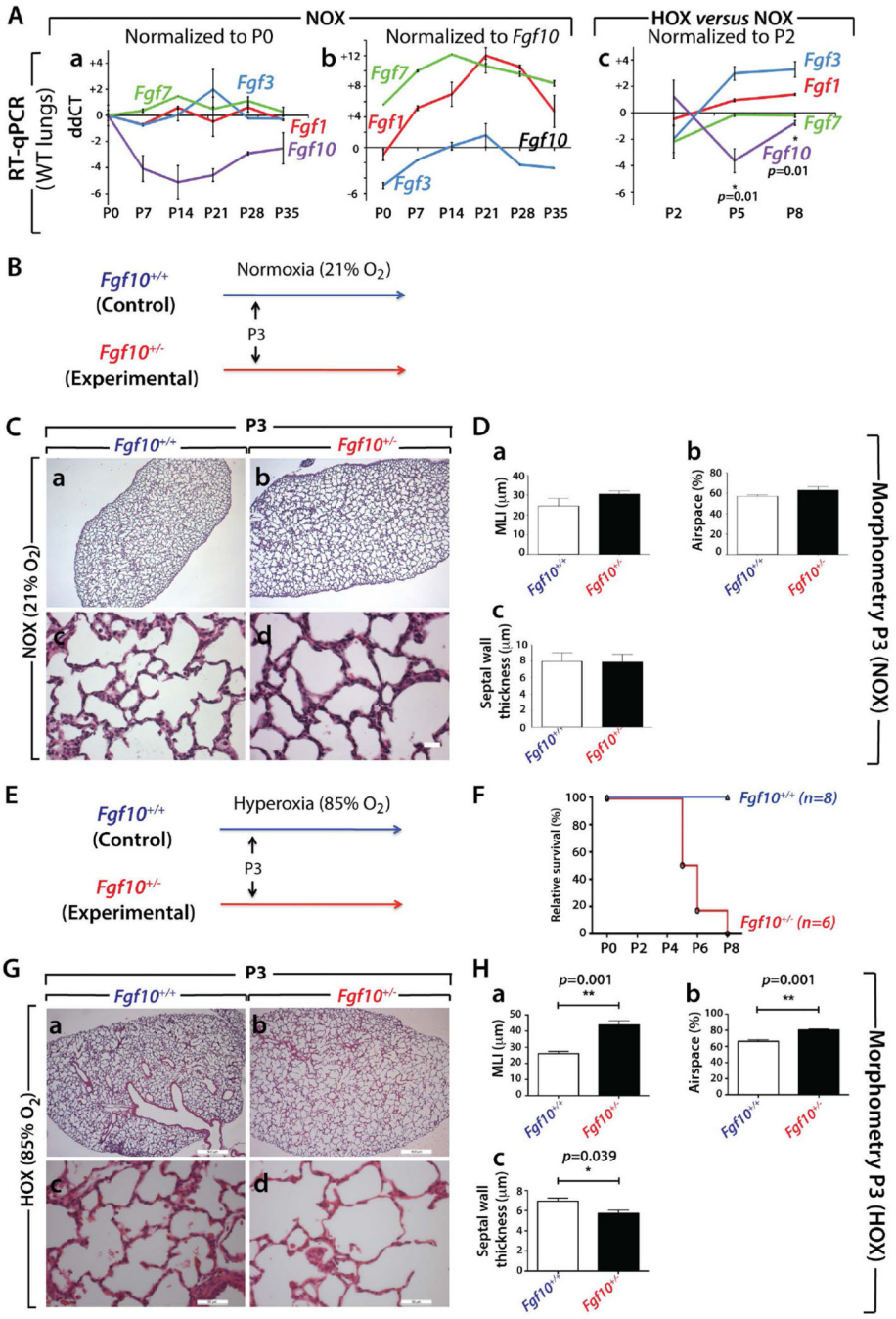


**Figure 1. Congenital *Fgf10* insufficiency leads to neonatal death upon hyperoxia injury**

(**A**) RT-qPCR for *Fgf1*, *3*, *7* and *10* in lungs at various postnatal stages in normoxia (NOX). (**a**) Normalization to P0 for each of the ligands indicates that *Fgf10* expression decreases postnatally compared to P0 and compared to the other ligands. (**b**) Normalization to *Fgf10* expression at each time point indicates that *Fgf1* and *Fgf7* are expressed at higher levels than *Fgf10*. (**c**) Comparison of Fgfr2b ligands in hyperoxia (HOX) *versus* NOX indicates that *Fgf10* is the only Fgfr2b ligand mRNA to decrease significantly upon HOX injury. (**B**) Experimental set-up for NOX of $Fgf10^{+/-}$ (experimental group) and $Fgf10^{+/+}$ (control

group) animals. (**C**) Haematoxylin/eosin staining of NOX exposed (**a,c**) control or (**b,d**) experimental lungs at P3. (**D**) Corresponding lung morphometric analysis. Note the absence of difference in (**a**) MLI, (**b**) airspace and (**c**) septal wall thickness. (**E**) Experimental set up for HOX of *Fgf10*$^{+/-}$ (experimental group) and *Fgf10*$^{+/+}$ (control group) animals. (**F**) Survival curve for HOX-exposed animals showing that all of the experimental animals died within 8 d, whereas all of the control animals survived. (**G**) Haematoxylin/eosin staining of HOX exposed (**a,c**) control or (**b,d**) experimental lungs at P3. (**H**) Corresponding lung morphometric analysis of HOX-exposed control and experimental animals. Note the increase in (**a**) MLI, (**b**) airspace and the decrease in (**c**) septal wall thickness. Scale bar for Ca,b: 500 μm, Cc,d: 50 μm, Ga,b: 500 μm and Gc,d: 50 μm

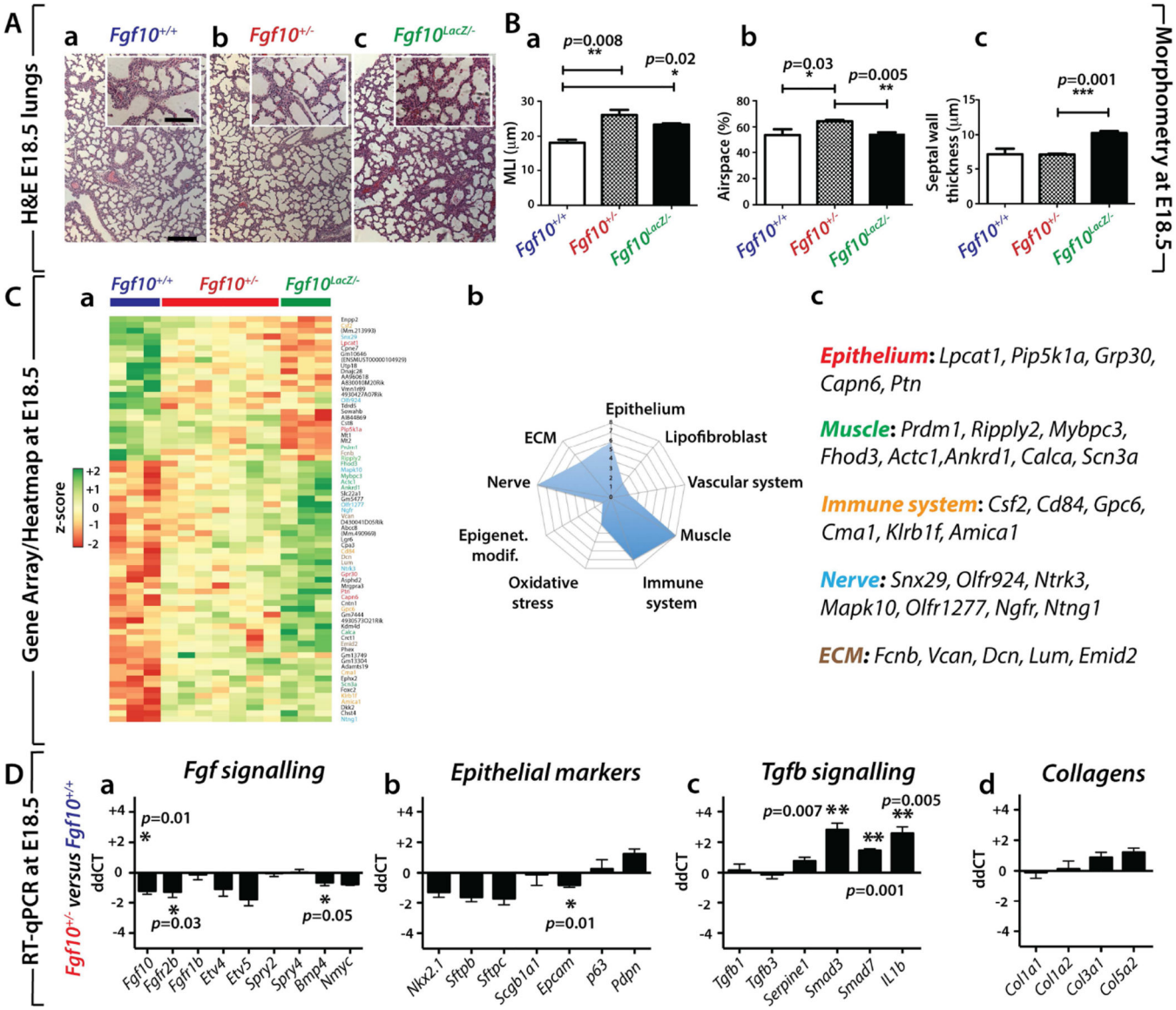


**Figure 2. E18.5 *Fgf10*$^{+/-}$ lungs display perturbed morphometry and impaired gene expression**

(A) Haematoxylin/eosin staining of (a) *Fgf10*$^{+/+}$ (b) *Fgf10*$^{+/-}$ (c) and *Fgf10*$^{(LacZ/-)}$ lungs at E18.5. (B) Morphometry of the lungs shown in (A). Note the increase in (a) MLI, (b) airspace and no change in (c) septal wall thickness in *Fgf10*$^{+/-}$ lungs compared to *Fgf10*$^{+/+}$ (C) (a) Gene array-based/Heat map analysis of the whole lung of E18.5 *Fgf10*$^{+/+}$, *Fgf10*$^{+/-}$ and *Fgf10*$^{(LacZ/-)}$ lungs indicating that *Fgf10* deficient lungs display an impaired pattern of gene expression compared to *Fgf10*$^{+/+}$ lungs (Please see Figure S2 for greater magnification). (b) Symbolic representation of the genes affected grouped by cell types or processes. (c) Some of the relevant genes pertinent for the Epithelium, Muscle, Immune system, Nerve and ECM are listed. (D) Expression analysis by RT-qPCR of genes belonging to (a) FGF signalling, (b) epithelial markers, (c) TGFβ signalling, (d) and collagens between E18.5 *Fgf10*$^{+/-}$ and *Fgf10*$^{+/+}$ lungs. Note the decrease in *Fgf10* signalling mRNAs *Fgfr2b* and *Bmp4*, the decrease in *Epcam* as well as the increase in Tgfb signalling mRNAs *Smad3*,

*Smad7*, *IL1b*. Collagen mRNA levels were not significantly different at this stage. Scale bar Aa–c: 125 μm inserts: 30 μm.

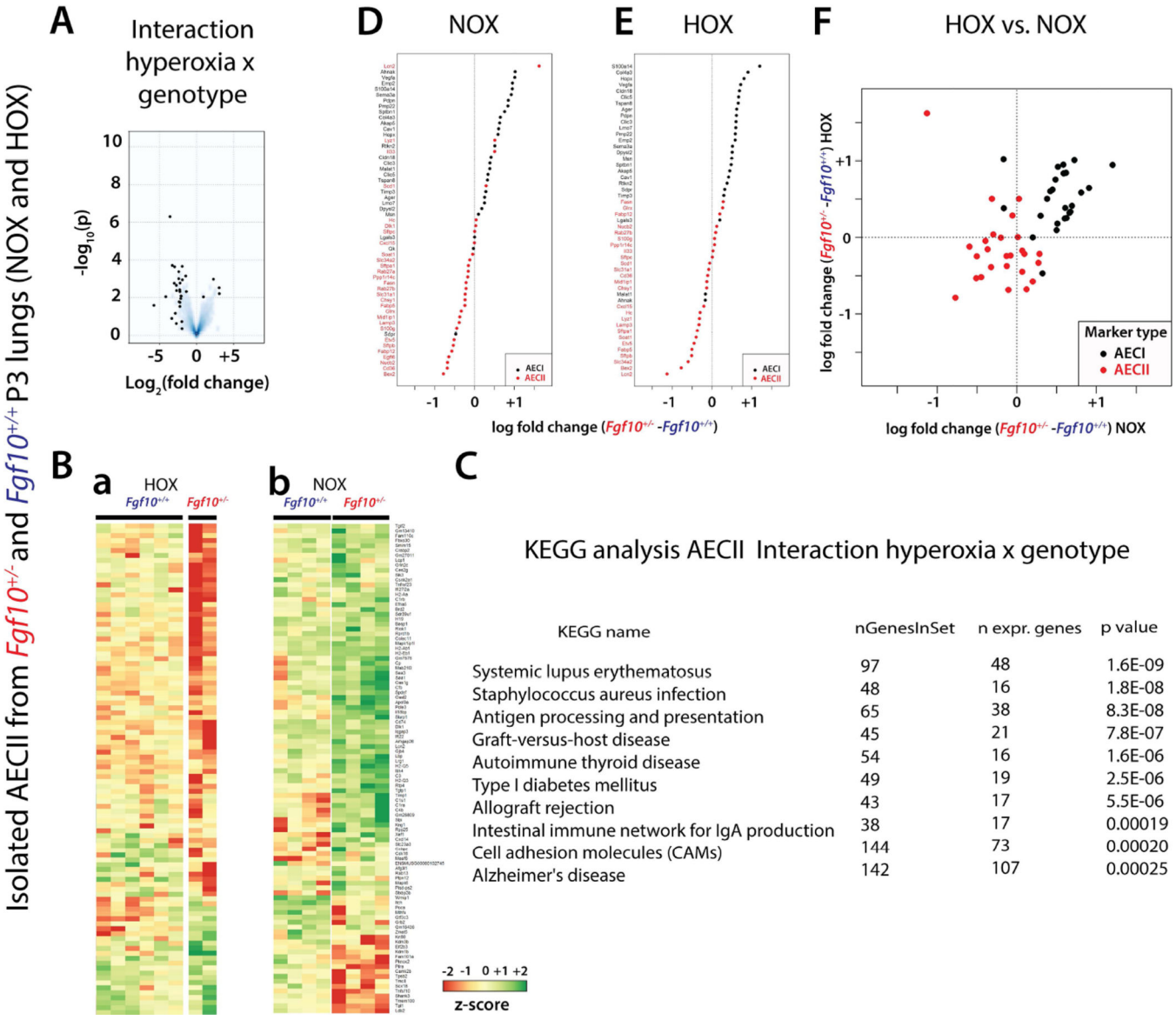


| KEGG name | nGenesInSet | n expr. genes | p value |
|---|---|---|---|
| Systemic lupus erythematosus | 97 | 48 | 1.6E-09 |
| Staphylococcus aureus infection | 48 | 16 | 1.8E-08 |
| Antigen processing and presentation | 65 | 38 | 8.3E-08 |
| Graft-versus-host disease | 45 | 21 | 7.8E-07 |
| Autoimmune thyroid disease | 54 | 16 | 1.6E-06 |
| Type I diabetes mellitus | 49 | 19 | 2.5E-06 |
| Allograft rejection | 43 | 17 | 5.5E-06 |
| Intestinal immune network for IgA production | 38 | 17 | 0.00019 |
| Cell adhesion molecules (CAMs) | 144 | 73 | 0.00020 |
| Alzheimer's disease | 142 | 107 | 0.00025 |

**Figure 3. Interaction "hyperoxia × genotype" analysis to identify the significant genes/pathways differentially affected by HOX in isolated AECII cells from WT and *Fgf10*$^{+/-}$ lungs at P3**

(A) Volcano plot. (B) Top 100 regulated genes in (**a**) HOX *versus* (b) NOX in AECII cells isolated from *Fgf10*$^{+/-}$ and WT mice (Please see Figure S5 for greater magnification). (C) KEGG analysis of the interaction "hyperoxia × genotype". (D) AECI and AECII gene-set analysis comparing AECII cells isolated from *Fgf10*$^{+/-}$ and WT lungs in NOX (Please see Figure S6 for greater magnification). (E) AECI and AECII gene-set analysis comparing AECII cells isolated from *Fgf10*$^{+/-}$ and WT lungs in HOX. (Please see Figure S6 for greater magnification). (F) AECI and AECII gene-set analysis in AECII cells isolated from *Fgf10*$^{+/-}$ *versus* WT lungs in HOX or NOX.

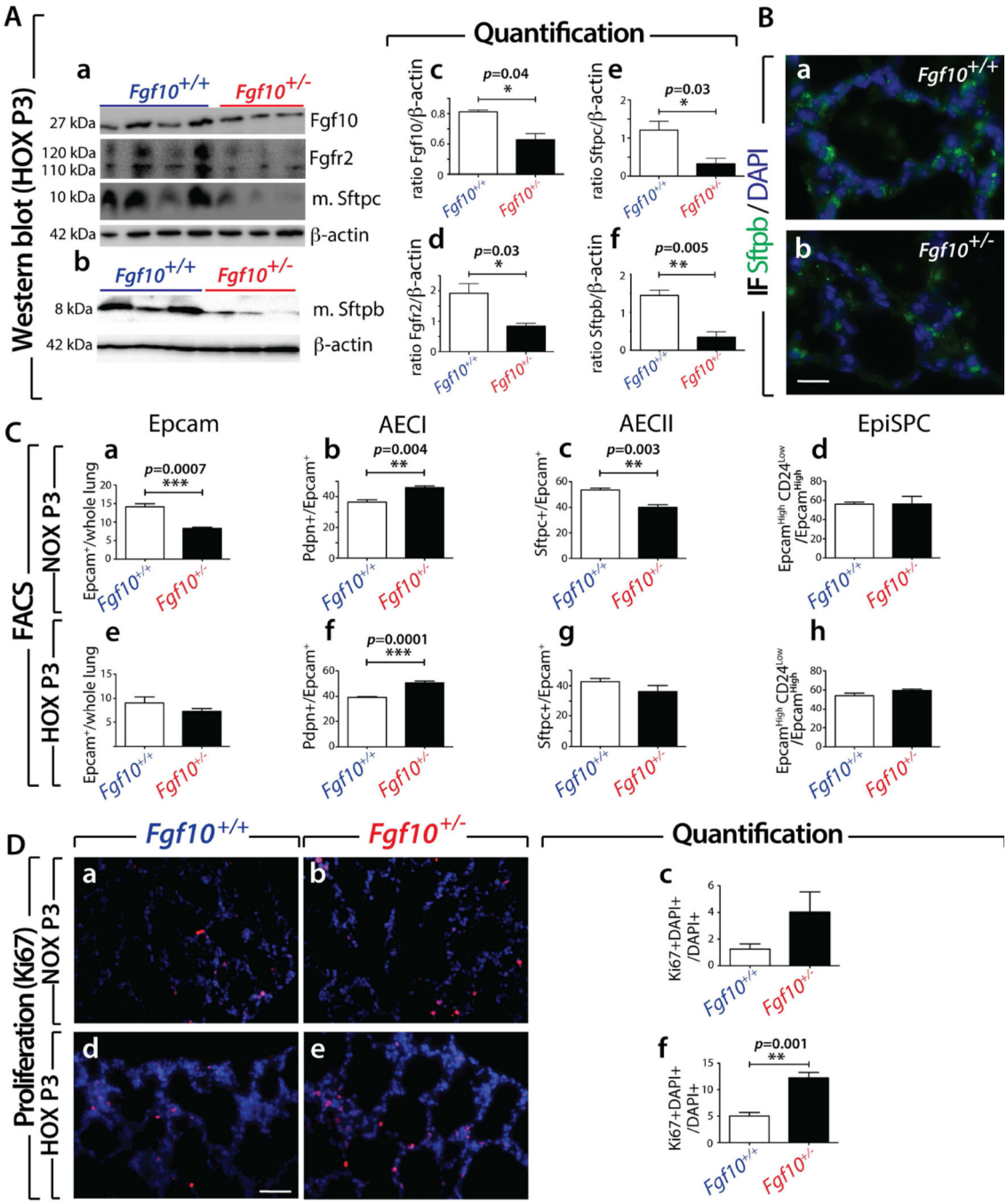


**Figure 4. *Fgf10*$^{+/-}$ lungs in the context of HOX exhibit less mature-Sftpc and mature-Sftpb**

(A) Western blotting analysis (whole lung homogenates) for (a) Fgf10, Fgfr2, mature-Sftpc and β-actin as well as (b) mature-Sftpb and β-actin on *Fgf10*$^{+/+}$ and *Fgf10*$^{+/-}$ lungs exposed to HOX at P3. (c–f) Quantification of bands using ImageJ software (b–d). (B) Immunofluorescence for Sftpb in P3 HOX *Fgf10*$^{+/-}$ and *Fgf10*$^{+/+}$ lungs. (C) Fluorescence Activated Cell Sorting in NOX (a–d) and HOX (e–h) of *Fgf10*$^{+/+}$ and *Fgf10*$^{+/-}$ P3 lungs for (a,e) Epcam, (b,f) AECI, (c,g) AECII and (d,h) Epithelial Stem Progenitor Cells (EpiSPC). (D) Ki67 labelling for proliferation in (a,b) NOX and (d,e) HOX for (a,d) *Fgf10*$^{+/+}$ and (b,e)

*Fgf10*$^{+/-}$ P3 lungs. (c,f) The Ki67+ fraction of cells in (c) NOX and (f) HOX. Note the increase in Ki67+ cells in the *Fgf10*$^{+/-}$ lungs exposed to HOX. Scale bar: Ba,b: 20 μm; Da,b,d,e: 50 μm.

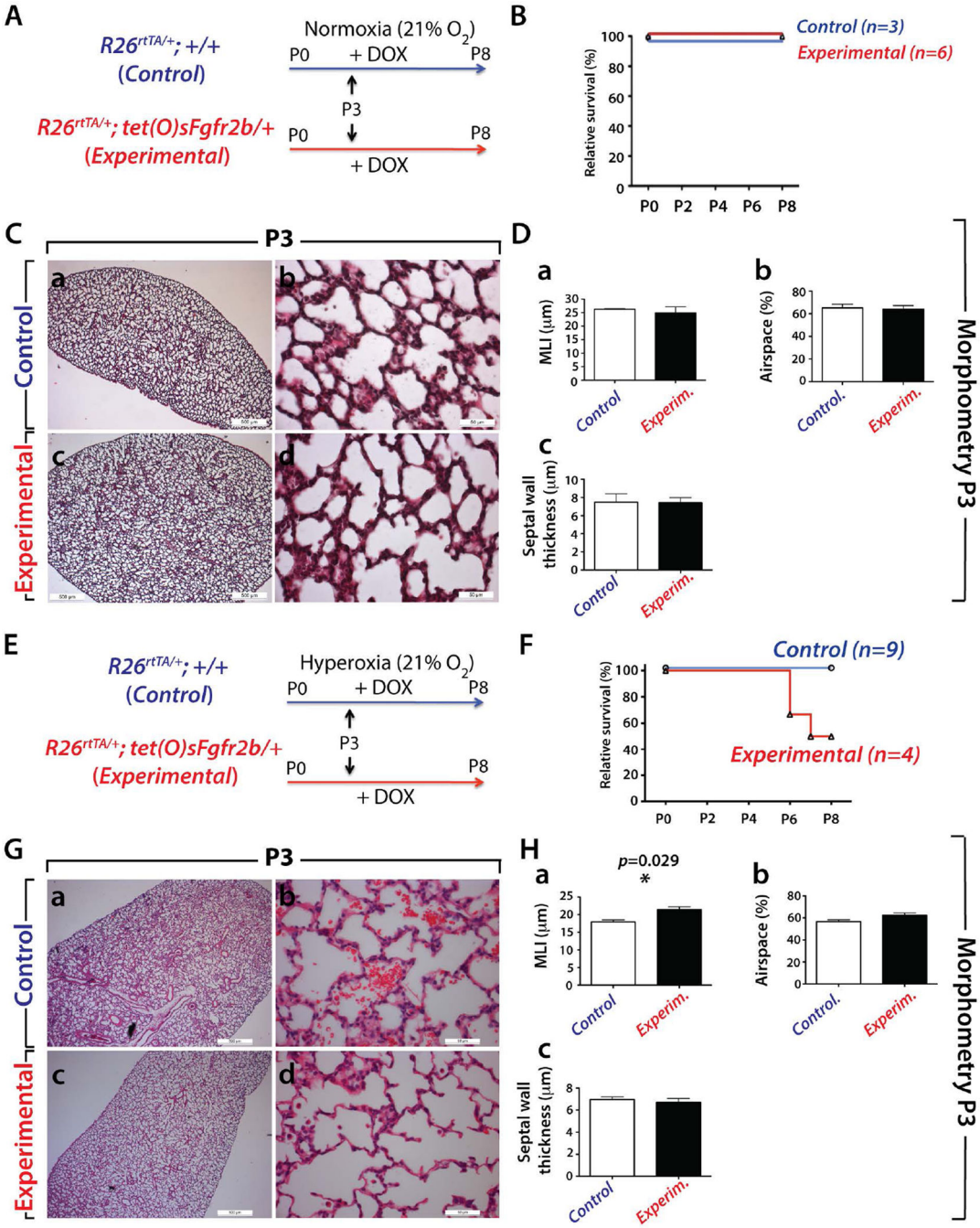


**Figure 5. Attenuation of Fgfr2b ligands postnatally in the context of HOX exposed pups leads to significant lethality**

(A) Experimental set-up for NOX of *R26rtTA/+; tet(O)sFgfr2b/+* (experimental group) and *R26rtTA/+; +/+* (control group) animals. Animals are fed with doxycycline-containing food to induce the dominant negative soluble Fgfr2b in the experimental group. (B) Survival curve for NOX exposed animals indicating that all experimental and control animals survive in NOX. (C) Haematoxylin/eosin staining of NOX exposed (a,b) control or (c,d) experimental lungs at P3. (D) Corresponding lung morphometric analysis. Note the absence of differences in (a) MLI, (b) airspace and (c) septal wall thickness. (E) Experimental set-up

for HOX of *R26rtTA/+; tet(O)sFgfr2b/+* (experimental group) and *R26rtTA/+; +/+* (control group) animals. (F) Survival curve for HOX exposed animals indicating that 50% of the experimental animals die within 8 days while all the control animals survive. (G) Haematoxylin/eosin staining of HOX exposed (a,b) control or (c,d) experimental lungs at P3. (H) Corresponding lung morphometric analysis of HOX exposed control and experimental animals. Note the increase in (a) MLI while (b) airspace and (c) septal wall thickness are not affected. Scale bar for Ca,c and Ga,c: 500 μm and Cb,d and Gb,d: 50 μm.

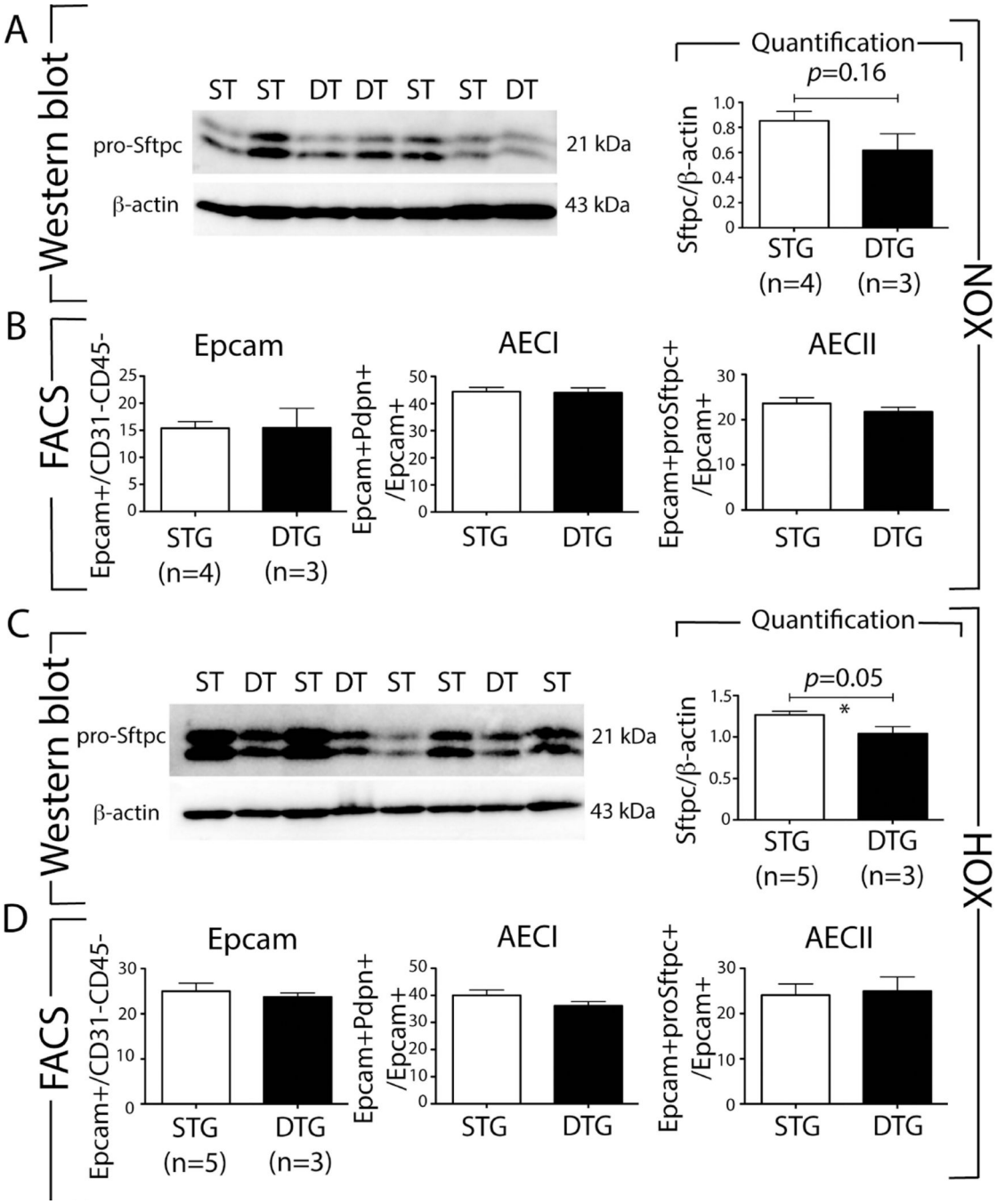


**Figure 6.** ***Rosa26rtTA/+;Tg(tet(o)sFgfr2b)/+ (DTG)*** **lungs in the context of HOX exhibit decreased Sftpc expression without quantitative change in the prevalence of Epcam, AECI and AECII cells**

(A) Western blot analysis for pro-Sftpc and β-actin of STG and DTG P3 lungs exposed to NOX. Quantification of the western blot results shows no difference between STG and DTG mice. (B) Fluorescence Activated Cell Sorting of cells from STG and DTG P3 lungs in NOX for Epcam, AECI and AECII cells. No quantitative changes are observed in NOX. (C) Western blot analysis for pro-Sftpc and β-actin on STG and DTG P3 lungs exposed to HOX. Quantification of the western blot results shows a significant decrease in Sftpc expression in DTG *versus* STG mice. (D) Fluorescence Activated Cell Sorting of cells of STG and DTG

P3 lungs in HOX for Epcam, AECI and AECII cells. No quantitative changes are observed in HOX.